# 5

# Self-Assembled Nanodot Fabrication by Using PS-PDMS Block Copolymer

Miftakhul Huda, You Yin and Sumio Hosaka
*Graduate School of Engineering, Gunma University*
*Japan*

## 1. Introduction

The downsizing of nanolithography technology has given great benefit on achieving faster, low power consumption, and high integrated structure of electronics devices. Therefore, this nanolithography technology has drawn many scientists and engineers to be involved and put their main goal on this field in many decades. To obtain nanostructures especially nanodot, there are many methods which have been developed. Before block copolymer self-assembly technique is presented, those methods to fabricate nanostructures are discussed. Those methods could be divided into 2 large categories. Those are top-down method and bottom-up methods. The methods to fabricate nanodot also could be divided into top-down and bottom-up methods. Top-down method patterns material at large scale by reducing its dimension to the nanoscale. Bottom-up methods arrange atoms or molecules to form nanostructures.

Top-down methods could be defined as patterning by scraping material into smaller dimension. The main representatives of top-down methods are lithography, Electron Beam (EB) Drawing, and Ion Beam technique. Many experiments in fabrication nanodots using these techniques have been reported.

In lithography technique, a beam of light (typically a UV light) passes through the mask and a lens, which focuses a designed pattern on photoresist (photosensitive coating of material) placed on a surface of a silicon wafer or film. Then, the exposed or the masked part of photoresist is removed leaving the desired pattern on silicon wafer or film depending on the characteristics of the used photoresist. To date, this technique has been widely used for fabricating nanoelectronics device. However, the dimension of nanopatterns which can be fabricated using this technique is limited by the wavelength of used light. Many improvements, including various technical improvements and modifications by using X-rays or extreme ultraviolet light, have been developed to reach resolution less than 20 nm. Therefore, those improvements make this technique rather expensive and increase its difficulties. Moreover, it seems that the resolution of nanopattern fabricated by lithography has reached near its limit.

Electron Beam Drawing or EB Drawing is the most potential candidate to replace current lithography technique. EB Drawing uses focused electron beam instead of light to bombard a thin resist layer on a surface of silicon or film followed by rinse process.

Depending on the characteristic of the resist, the bombarded parts will remain or be removed leaving nanopattern in accordance with CAD design. Hosaka and other researchers have reported the fabrication of nanodots with density more than 1 Tbit/in.$^2$ or pitch of nanodots less than 25 nm. According to the theory, it is possible to fabricate nanodots with pitch less than 3-5 nm or density up to 83 Tbit/in.$^2$. However, many issues must be solved first including the used resist, proximity effect, focusing electron beam, and other technical problems. In Industry, EB Drawing is often used as application to fabricate a mask or template for lithography or stamper processes. However, EB Drawing is unlikely to be used in fabricating nanostructures at large and rapid scales due to very high cost, low throughput, and consuming high energy.

Ion Beam technique has similar principal with EB Drawing. Ion Beam technique uses ion beam instead of electron. One of techniques in this category, Ion Projection Lithography (IPL) has the complete absence of diffraction effects coupled with ability to tailor the depth of ion penetration to suit the resist thickness or the depth of modification. This characteristic gives advantage to pattern a large area in a single brief irradiation exposure without any wet processing step. While Focused Ion Beam (FIB) can produce master stamps in any material. 8 nm lines written into a multilayer sample of AlF3/GaAs have been succeeded fabricated using FIB. Although this technique has now breached the technologically difficult 100 nm barrier, and are now capable of fabricating structures at the nanoscale, the obstructions for fabricating high area and high density nanopattern with low cost production still remain. However, Ion Beam techniques are combined with nanoimprinting and pattern transfer for mass production.

In bottom-up methods, atoms or molecules are arranged to form higher dimension of nanostructures by mechanical/physical, chemical, or self-assembly processes. Bottom-up methods include nanofabrication using Scanning Probe Microscope, Chemical Vapour Deposition (CVD), and self-assembly process. Compare to others, self-assembly process has great advantages on high throughput and low cost. Among self-assembly techniques, however, block copolymer self-assembly technique is likely to be the most applicable in nanoelectronics device industry.

In general, nanofabrication techniques using SPM have been used for direct writing of nanostructures through material modification, deposition, and removal. The scanning tip of SPM acts as mechanical, thermal, and/or electric source to initiate and perform various physical and chemical for forming nanostructures. There are two major technologies within SPM which are used: scanning tunnelling microscopy (STM) and atomic force microscopy (AFM). Nanofabrication using STM has demonstrated manipulation of resist surface at atomic scale resolution to form sub-nano scale of pattern. Very low throughput, limited resist, and the requirements of high-vacuum and controlled environment have left this technique in laboratory. Using AFM, nanofabrication can be performed at normal ambient environment so more resist material can be used and the process is easier. However, the resolution of fabricated nanopatterns is limited by the size and by the shape of cantilever tip, and the tip writing speed (rate) is still need to be improved to increase its low throughput.

The product of Chemical Vapour Deposition (CVD) is almost deposit materials such as film in various forms with high purity and high performance. Some nanostructures fabrications are reported. However, the issue of order, alignment, and shape controls of nanostructures is still

need to be resolved. Many process modifications and material selection in CVD are important to obtain applicable products. Therefore, we will not discuss this technique in detail.

The development of semiconductor technology has reached unprecedented level. The high-cost and limitation of nanofabrication using top-down methods yield the expectation of other methods increasing. Self-assembly technique offering low cost and ease process has attracted in recent few years. As an alternative technique, the self-assembly of block copolymer (BCP) offers a simple and low-cost process to form large-area periodic nanostructures, giving it great potential for application to fabricate patterned media that will be used for the next-generation magnetic recording. It have also been previously demonstrated that the self-assembled nanostructures have the potential to function as etching masks or templates in nano-patterned lithography. Aissou et. al. used BCP thin films as deposition and etching mask to fabricate silicon nanopilllar arrays with dimension and periodicities which are difficult using conventional technologies like optical, e-beam lithography and etching process. Therefore, this finding has increase possibility of BCP self-assembly technique to be utilized as an application for fabricating electronic devices.

Another significant achievement in the research to increase possibility of BCP self-assembly technique was reported recently. Bita et. al. used a topographical graphoepitaxy technique for controlling the self-assembly of BCP thin films that produces 2D periodic nanostructures with a precisely determined orientation and long-range order. The experiment showed that designated nano guide post formed by e-beam lithography, which is functionalized as surrogate nanodots of BCP self-assembly nanodots, effectively controlled nanodots in forming long range ordered nanodot pattern. In our research, Hosaka et. al. demonstrated the possibility of forming long-range ordering self-assembled nanodots array using mixing guide posts those are nanodots guide post and nano guide line fabricated by e-beam lithography. Recently, techniques to control orientation and periodicity of self-assembled nanostructures are well established by designated template, chemical modification, electric induction, modifying self-assembly medium, etc.

Two developed achievements in BCP self-assembled pattern-transfer and controlling periodicity and orientation of BCP self-assembled nanostructures have attracted many researchers and engineers in lithography field. This method offers an applicable new technique as strong candidate to replace current photolithography technique.

## 2. Self-assembly of block copolymer

A block copolymer consists of two or more polymeric blocks which are chemically or covalently bonded. In the melt condition, they are driven to segregate into various nanostructures by the repulsion of the immiscible blocks, almost in the case of a blend of immiscible homopolymer blocks. This segregation process, which gives result in microphase separation, is defined as self-assembly of block copolymer. In this far simpler case of block copolymer which consists of two homopolymer blocks, A and B, the nanostructure (phase) behaviour of BCP self-assembly process can be easily managed by simply varying parameters of the block copolymer, such as the total number of segments N, the volume fraction f of BCP component, the Flory-Huggins segmental interaction parameter $\chi$, and the molecular architecture of the BCPs. Block copolymer consisting two homopolymer block is

also called as diblock copolymer. The Flory–Huggins equation describes approximately how these parameters affect the free energy of a blend:

$$\frac{\Delta G_{mix}}{k_b T} = \frac{1}{N_A}\ln(f_A) + \frac{1}{N_B}\ln(f_B) + f_A f_B \chi \quad (1)$$

The first two terms correspond to the configurational entropy of the system, and can be regulated via the polymerization chemistry to change the relative lengths of the chains and fractions of A versus B block of polymer. In the third term of (1), $\chi$ is associated with the non-ideal penalty of A–B monomer contacts and is a function of both the chemistry of the molecules and temperature. In general,

$$\chi = \frac{a}{T} + b \quad (2)$$

where a and b are experimentally obtained constants for a given composition of a particular blend pair. Experimentally, χ can be controlled through temperature. Unlike macrophase separation in blends, the connectivity of the blocks in block copolymers prevents complete separation and instead the block copolymer chains organize to put the A and B portions on opposite sides of an interface. The equilibrium nanodomain structure must minimize unfavorable A–B contact without over-stretching the blocks. The strength of segregation of the two blocks is proportional to χN. A symmetric diblock copolymer is predicted to disorder (or pass through its order–disorder temperature (ODT)) when $\chi N < 10$. Below the ODT and when the volume fraction of block A ($f_A$) is quite small, it forms spheres in a body-centered cubic (BCC) lattice surrounded by a matrix of B. As $f_A$ is increased towards 0.5, the minority nanodomains will form first cylinders in a hexagonal lattice, then a bicontinuous double gyroid structure, and finally lamellae. This phenomenon is described in Fig. 1

Mean-field phase diagram in Fig. 1 shows the theory of BCP self-assembled nanostructures. The X-axis corresponds to the volume fraction of block copolymer $f_A$, and the Y-axis corresponds to the product of the Flory-Huggins parameter χ and the total number of segments N. As shown in Fig. 1, nanostructures such as spherical, cylindrical, or lamellar structures can be obtained by changing the volume fraction f of BCP components. Other structures such as gyroid and close-packed sphere (CPS) structures are also observed on a small range of certain BCP composition. Fig. 1 also shows that the product of χN in the Y-axis is relatively equivalent to the self-assembled nanostructure size due to the total number of BCP segments N equal to the size of BCP. This means that to obtain smaller nanostructure by using the same BCP, it is necessary to adopt the same BCP with lower total number of BCP segments N. In experiment, we chose BCP with low molecular weight to obtain smaller nanodots.

In this chapter, fabrication of nanodots using block copolymer technique will be discussed. The discussion is based on experiment of block copolymer self-assembly technique using Polystyrene-Poly(dimethylsiloxane) (PS-PDMS) block copolymer. We demonstrated the nanodot pattern fabrication using polystyrene-poly(dimethyl siloxane) (PS-PDMS) BCPs with three different molecular weights of 30,000-7,500, 13,500-4,000, and 11,700-2,900. We chose PS-PDMS because of its high etch selectivity and its high Flory-Huggins parameter χ. PS-PDMS block copolymers have been demonstrated to have a high etch selectivity between the two kinds of blocks because organic PS block can be easily etched while Si-containing

organometallic PDMS block as nanodots shows high endurance to etching. PDMS which contains Si will form a material with property like silica when etched by oxygen ($O_2$) gas. This result implies on high etch selectivity between PDMS and PS domain. Its high etch selectivity will give advantage in subtractive pattern transfer while its Flory-Huggins parameter $\chi$ implies its advantage in obtaining very fine nanodot pattern with pitch size at sub-10 nanometers. In practice, PS-PDMS has economic advantages since the annealing temperature and annealing time, which is necessary to promote self-assembly process, are relatively less compare to BCP which is used in conventional research such as PS-PMMA. It was also reported that vapour solvent-annealing treatment was demonstrated to promote self-assembly process of PS-PDMS.

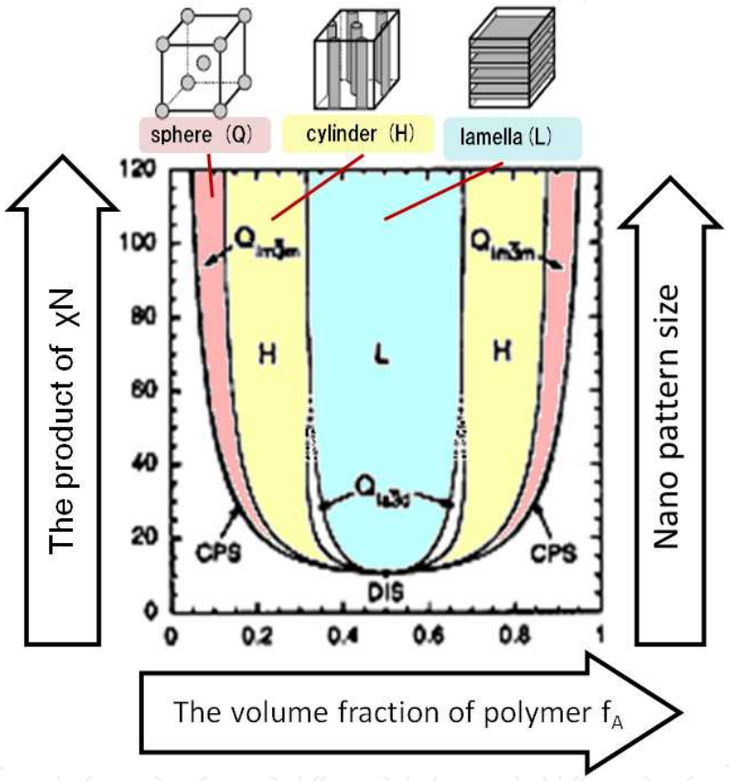


Fig. 1. Mean-field phase diagram for BCP melts shows the theory of BCP self-assembled nanostructures. The images in above diagram describe schematics of thermodynamically stable block copolymer phases.

## 3. Experimental method

In this work, we adopted spherical morphology PS-PDMS BCPs with molecular weights of 30,000-7,500, 13,500-4,000, and 11,700-2,900 and minority block volume fraction $f_{PDMS}$ of 20%, 24%, and 20.9%, respectively. Fig. 2(a) schematically shows the experimental process that is used to form self-assembled nanodots. We dissolved PS-PDMS in a certain solvent to obtain PS-PDMS solutions with a weight concentration of 2%. Then, PS-PDMS solutions were spin-coated onto silicon substrates of 1 $cm^2$ and annealed at 170°C in a $N_2$ atmosphere or vacuum for 11 hours.

Fig. 2(b) illustrates the process of self-assembly using PS-PDMS. The spherical PDMS nanodots formed by microphase separation are shown here. Fig. 2(b-1) shows a spin-coated PS-PDMS film sample. After annealing, a very thin PDMS layer preferentially segregates at the air/polymer interface because of the low surface energy of PDMS. This produces the structure schematically shown in Fig. 2(b-2). We conducted reactive ion etching (RIE) using $CF_4$ gas to remove the very thin top PDMS layer. Finally, we conducted RIE using $O_2$ gas in order to remove the PS domain and to form the nanodot pattern. This $O_2$ plasma etching also causes the Si-containing PDMS domain partly oxidized, leaving a material with properties similar to silica that is robust for subtractive pattern transfer. RIE was conducted for all samples in the same condition. The etched nanodots are schematically shown in Fig. 2(b-3).

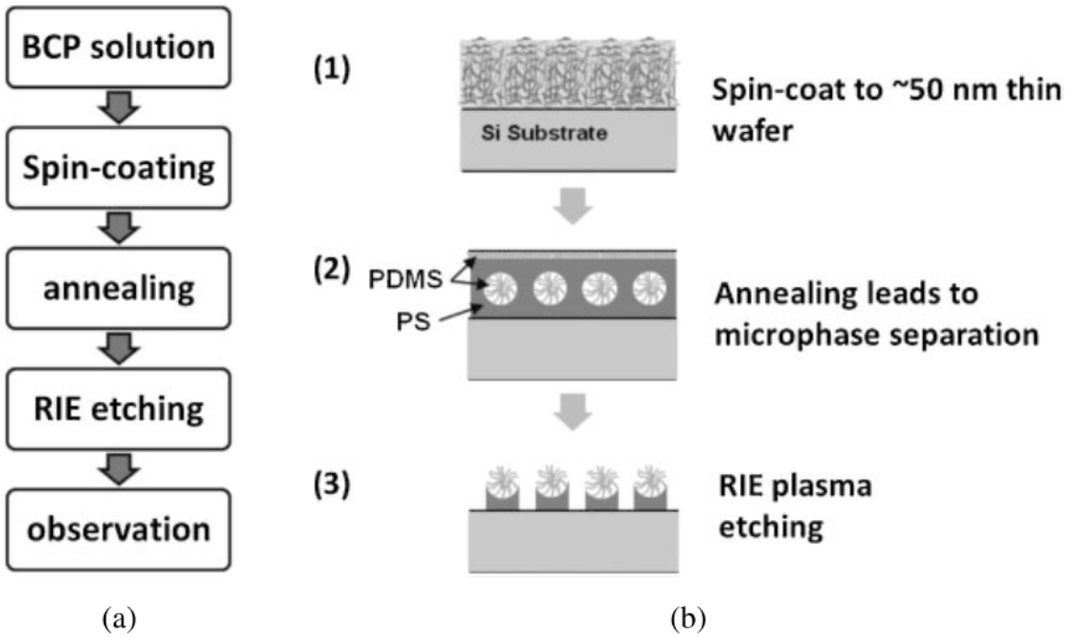


Fig. 2. Self-assembly process of BCP: (a) experimental process flow and (b) self-assembly process of PS–PDMS BCP.

We used a high-resolution scanning electron microscope (SEM; JEOL JSM6500F) to observe the PS-PDMS films after etching process. We used atomic force microscopy (AFM) to measure the thickness of the PS-PDMS film. The PS-PDMS films were partly removed, and the difference in height was measured. This measurement was conducted before annealing was applied on the sample.

## 4. Result and discussion

In our first experiment, we chose PS-PDMS with molecular weight of 30,000-7,500 and minority block volume fraction $f_{PDMS}$ of 20%. In experiment, this PS-PDMS formed nanodots pattern with optimal size approximately 33 nm in pitch and 23 nm in diameter. Then, we selected PS-PDMS with lower molecular weights of 13,500-4,000 and 11,700-2,900 to obtain smaller nanodots.

### 4.1 Formation of nanodots formed by PS-PDMS 30,000-7,500

Firstly, we investigated the dependence of self-assembly process on concentrations. Figs. 3(a), (b), and (c) show SEM images of fabricated nanodots by PS-PDMS self-assembly with different concentrations (wt/wt) of 1%, 2%, and 3%, respectively. According to PS-PDMS self-assembly process shown in the Fig. 2(b), nanodot-shaped patterns and the surrounding regions in Fig. 3 are believed to correspond to unetched-PDMS domain and bared Si substrate after PS matrix was removed by $O_2$ RIE. It can be seen from the SEM image of Fig. 3 (b) that the nanodots look darker than the surroundings, compared with Figs. 3(a) and 3(c). The main reason for this should be the so-called edge effect that more secondary electrons are produced at edges and thus the regions at edges look brighter than other regions. The relatively narrow gap between nanodots shown in Fig. 3(b) enhances the edge effect, making the gaps look brighter than nanodots. On the contrary, the gaps are relatively wide for formed nanodots shown in Figs. 3(a) and 3(c) so the gap regions reasonably look dark although the dark nanodots are surrounded by brighter edges.

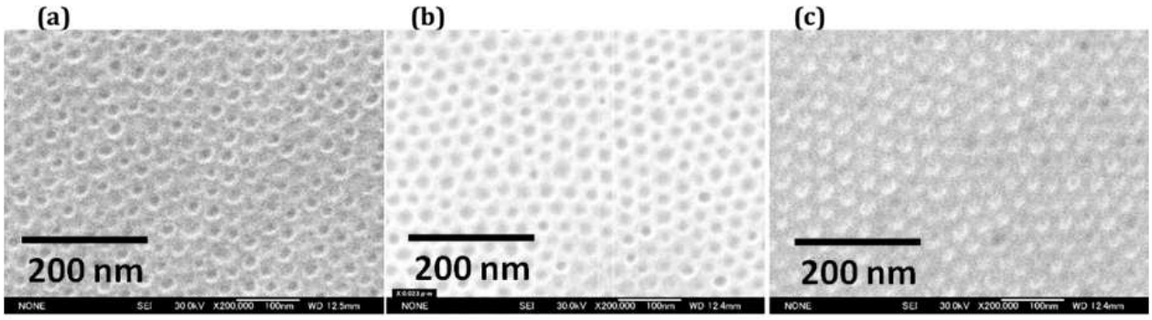


Fig. 3. Fabricated nanodots pattern using PS-PDMS block copolymer with molecular weight 30,000-7,500, which dissolved onto different concentrations those are 1%, 2%, and 3% corresponding to images (a), (b), and (c), respectively.

The average nanodot size in diameter and pitch size are summarized in Fig. 4. As shown in Fig. 4, the smallest pitch size of nanodots, around 33 nm, was achieved for the concentration of 2%. Much larger pitch size, around 41 nm, was observed for the concentration of 1%. The diameters of nanodots for each concentration are almost similar, as small as around 23 nm. This result makes us conclude that 2% in concentration is the most suitable concentration to optimize the pitch size of nanodots into the smallest, which indicates high density of nanodots.

Fig. 5 shows the SEM images of fabricated nano-patterns as a function of dropped volume. Figs. 5 (a), (b), and (c) show the SEM images of these patterns formed by dropping different volumes of 10, 20, and 40 μL onto Si substrate with a size of 1 $cm^2$, respectively. Only 2% PS-PDMS solution was used here. The enhanced edge effect can be also observed in Fig. 4(c) when the gap between nanodots is relatively narrow. When the dropped volumes of PS-PDMS solution are 20 μL or 40 μL, the morphologies of PS-PDMS self-assembly pattern are spherical structure. The morphology of PS-PDMS self-assembled pattern becomes fingerprint-like cylindrical structure when the dropped volume of PS-PDMS solution was reduced to 10 μL. The width of the cylindrical structure is around 16 nm, similar to our experimental result of PS-PDMS self-assembly with a molecular weight of 13,500-4,000.

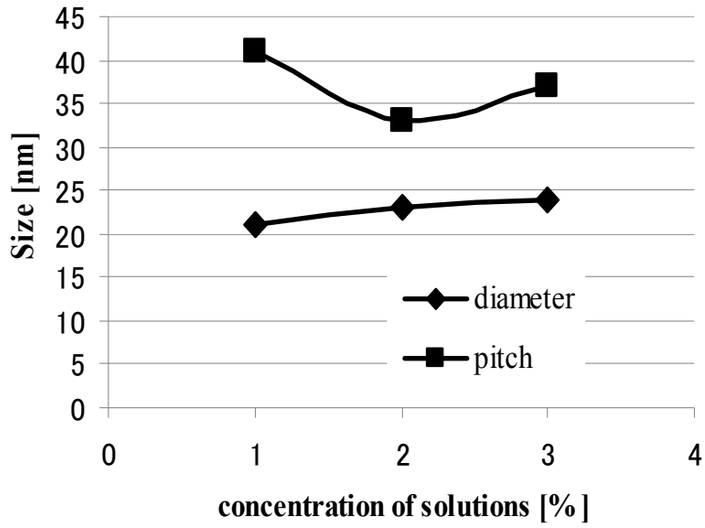


Fig. 4. Relation between nanodot size and concentration.

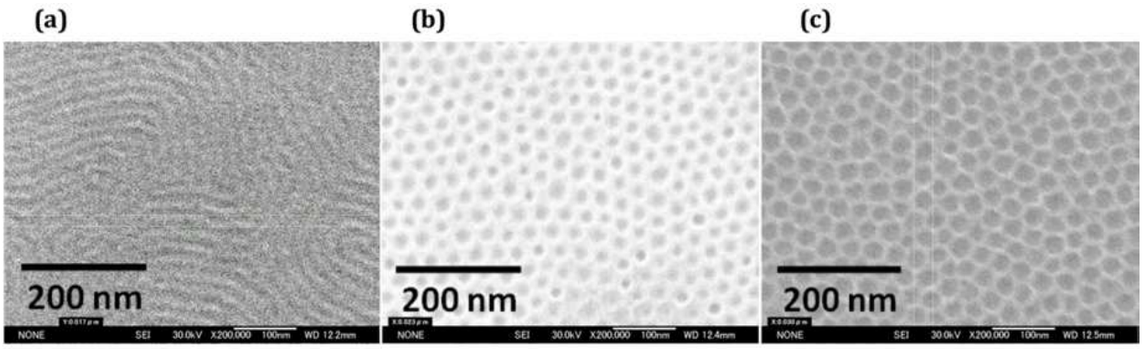


Fig. 5. Fabricated nanodots pattern using 2% solution of PS-PDMS block copolymer which is dropped with different volume onto 1 cm² silicon substrates. (a-c) 10, 20, and 40 μL, respectively.

The fewer the volume of solution is dropped, the thinner the layer of PS-PDMS is obtained on substrate. The thinness of PS-PDMS when the dropped volume is as little as 10 μL makes the two blocks of PS-PDMS block copolymer difficult to form spherical structure in the microphase separation process and cylinder which is parallel to the substrate tends to be formed. We believe that this phenomenon should be related to the lowest system energy. Forming nanodots for the little dropped volume must require higher energy than forming cylindrical structures. We summarized this tendency from Fig. 5 into graph shown in Fig. 6.

Fig. 6 also shows that there is correlation between the dropped volume of PS-PDMS block copolymer solutions and the size of formed nanodots. Since the dropped volume of PS-PDMS block copolymer solutions is corresponding to the thickness of PS-PDMS block copolymer layer, we believe that the size of nanodots can be controlled simply by dropping the most proper volume of block copolymer solutions. The thicker the PS-PDMS block copolymer layer is, the bigger the size of the formed nanodots is, although the size of nanodots is limited by the size of nanodot pitch.

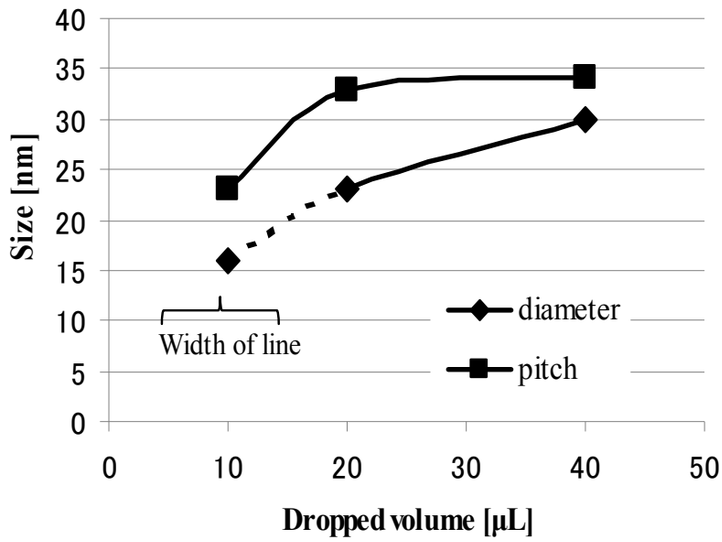


Fig. 6. Relations between the dropped volume of PS-PDMS solution and the size of nanodots. The dashed line indicates that the pattern morphology alters into random line.

### 4.2 Formation of smaller nanodots

In our first experiment, we used PS-PDMS which has molecular weight of 30,000-7,500 and minority volume fraction $f_{PDMS}$ of 20%. By optimizing experimental parameters, we succeeded in forming nanodot pattern with the pitch of nanodots as small as approximately 33 nm and the diameter of nanodots as small as 23 nm. In order to obtain smaller nanodots pattern, it is necessary to use BCP with less molecular weight and to keep the value of BCP's minority volume fraction according to the mean-field phase diagram for block copolymer melts. Therefore, we adopted two PS-PDMS BCPs which have molecular weights of 13,500-4,000 and 11,700-2,900 and minority block volume fractions $f_{PDMS}$ of 24% and 20.9%, respectively.

PS-PDMS has high Flory-Huggins parameter $\chi$ of 0.26. In the strong segregation of BCP such as PS-PDMS with a molecular weight of 30,000-7,500 and with $\chi N$ value of 101.2 (the molecular weights of styrene and dimethyl-siloxane blocks are 104.15 and 74.15, respectively), the pitch size of self-assembled nanodots is given by a formula below.

$$\text{Pitch} = aN^{\frac{2}{3}}\chi^{\frac{1}{6}} \tag{3}$$

where a is segment length. To predict the pitch size of PS-PDMS with molecular weights of 13,500-4,000 and 11,700-2,900, we used formula (3) by assuming that the estimation was done with the following two conditions being met. The first condition was that the segment lengths of the two adopted PS-PDMS are near the segment length of PS-PDMS with molecular weight of 30,000-7,500. The second was that both should promote microphase separation in the strong segregation. The prediction for the pitches of nanodots is shown in Fig. 7. It was predicted that PS-PDMS BCPs with molecular weights of 13,500-4,000 and 11,700-2,900 would form nanodots with pitch sizes as small as 24.3 nm and 17.5 nm, respectively.

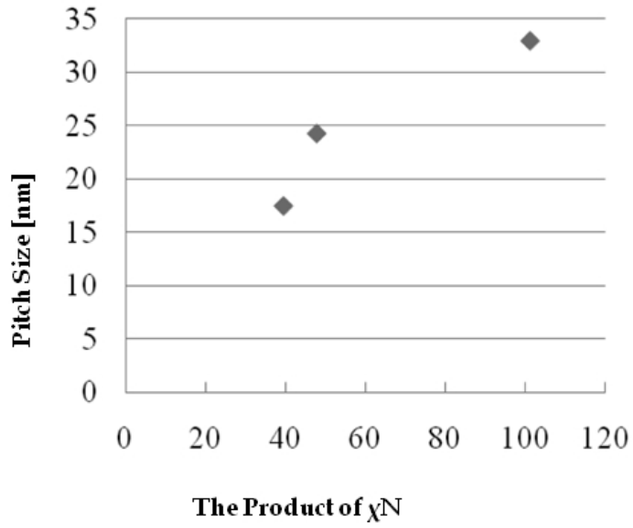


Fig. 7. The prediction of nanodots pitches of PS–PDMS BCPs with molecular weights of 30,000–7,500, 13,500–4,000, and 11,700–2,900.

### 4.3 Formation of nanodots formed by PS-PDMS 13,500-4,000

Fig. 8 shows SEM images [Fig. 8(a)] of self-assembled nanopatterns using PS-PDMS BCP with molecular weight of 13,500-4,000 and the corresponding schematic cross-section images

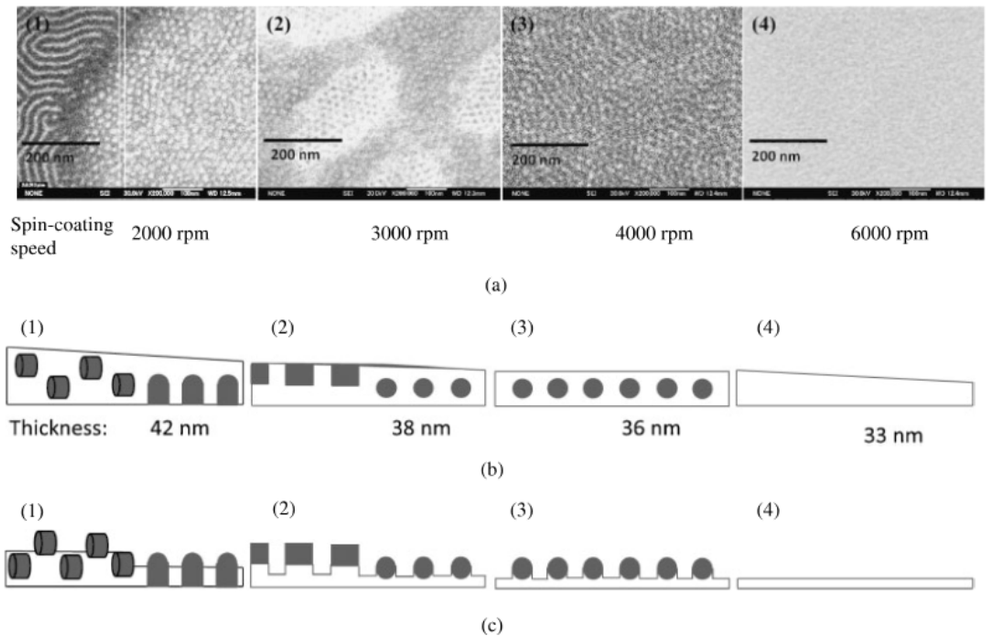


Fig. 8. (a) SEM images of self-assembled nanopatterns using PS–PDMS BCP with the molecular weight of 13,500–4,000 and the corresponding cross- section images of their schematic height profile. Images (1)–(4) show SEM images of nanopatterns when the spin-coating speed was changed to 2000, 3000, 4000, and 6000 rpm, respectively. (b, c) Schematic cross-section images of the correlating film height profile: (b) before etching and (c) after etching.

of the film height profile before [Fig. 8(b)] and after [Fig. 8(c)] etching process. Fig. 8(a) shows SEM images of self-assembled nanopatterns when the spin-coating speed changed to (1) 2000, (2) 3000, (3) 4000, and (4) 6000 rpm. All these images were taken on samples after $O_2$ plasma etching had been conducted on samples. The thickness of the PS-PDMS films, which formed before etching process, decreased with the increase of the spin-coating speed, as shown in Fig. 8(b). The thickness of the PS-PDMS films varies with spin-coating speed, and it is possible to obtain the optimum thickness for self-assembly by changing the spin-coating speed. Fig. 8(c) shows the schematic cross-section images of the film height profile after etching process, the numbers correspond to those of Figs. 8(a) and 8(b).

When the spin-coating speed was 2000 rpm, the thickness of the PS-PDMS film was 42 nm and the self-assembled nanostructure of the PDMS cylinders that was perpendicular and parallel to the substrate surface was obtained, as shown in Fig. 8(a-1). The direction of the parallel cylinders was partially orientated. According to our analysis, the width and pitch of the cylinders were 12 and 22 nm, respectively. However, the PDMS cylinders perpendicular to the substrate surface looked like nanodots when observed by SEM. The diameter and pitch of these nanodots were 12 and 22 nm, respectively.

When the spin-coating speed was 3000 rpm, the thickness of the PS-PDMS film was 38 nm, and self-assembled nanodots and nanoholes as a result of the semi-perforated lamella nanostructure were obtained. The brighter dots, which are surrounded by the darker region, are nanodots, and the darker dots in the brighter region are nanoholes. According to our analysis, the diameter and pitch of both nanodots and nanoholes were 12 and 22 nm, respectively. This result is shown in Fig. 8(a-2).

When the spin-coating speed was 4000 rpm, the thickness of the PS-PDMS film was 36 nm, and self-assembled nanodots were formed. The diameter and pitch of the nanodots were roughly 12 and 22 nm, respectively. This result is shown in Fig. 8(a-3).

When the spin-coating speed was increased to 6000 rpm, the thickness of the film decreased to 33 nm and no nanodots formed. This result is shown in Fig. 8(a-4).

The uniformity of the nanodots on a large area was also investigated. SEM images were randomly taken on a 1 $cm^2$ silicon substrate after etching process. The nanodot arrays formed uniformly when a 36-mm thick PS-PDMS film was formed with a spin-coating speed of 4000 rpm.

As shown in Fig. 8(a), the self-assembled nanostructures obtained when using PS-PDMS with molecular weight of 13,500-4,000 are not morphologically stable. We believe that this phenomenon occurred because the value of the PDMS fraction of this PS-PDMS is near the value of that which assembled into the cylinder nanostructure. This hypothesis also applies to the self-assembled nanostructure, which consists of cylinders perpendicular and parallel to the substrate surface, and was formed using PS-PDMS with molecular weight of 13,500-4,000 as shown in Fig. 8(a-1).

We describe the formed nanostructures when using PS-PDMS with molecular weight of 13,500-4,000, which change systematically as a function of the gradually changing film thickness in Fig. 8(b) (before etching) and in Fig. 8(c) (after etching), respectively. The darker regions indicate the PDMS block domains. When the film thickness was 42 nm, the hybrid nanostructure of the PDMS cylinders, which are perpendicular and parallel to the substrate

surface, were formed. This corresponds to the experimental result in Fig. 8(a-1). When a thinner film thickness of 38 nm was spin-coated, nanodots and semi-perforated lamella were formed. At the semi-perforated lamella, the minority block of PDMS fills the lamella domain at the surface of film, which is perforated by the majority block of PS filling it below. The short duration of $CF_4$ etching, however, was not enough to remove the minority block of PDMS at the surface. The remaining PDMS domains acted as a mask when the RIE etching of $O_2$ was conducted to remove the PS domain, which caused nanohole structures to be formed. This corresponds to the experimental result in Fig. 8(a-2), where the nanodots are shown as brighter dots and the nanoholes are shown as darker dots. Those results are consistent with a report by A. Knoll et al. that film thickness affects the formed nanostructures, which are determined by an interplay between surface field and confinement effect. The obtained nanostructures of cylinder-forming block copolymer were confirmed by experimental results and simulation using dynamic density functional theory.

When the optimum thickness of the PS-PDMS film was achieved, self-assembled nanodots were able to form on a large area, as shown in Fig 8(a-3). In the present experiment, the optimum thickness is 36 nm to form one nanostructure of nanodots, as described in Fig. 8(b-3). When the thickness of the film is less than the optimum thickness, no nanostructure is formed, as shown in Fig. 8(b-4). This corresponds to the experimental result in Fig. 8(a-4) when the film thickness was 33 nm. We believe that the confinement effect and the block length factor of PS-PDMS prevented microphase separation, and caused either a disordered phase or a lamellar wetting layer, which is formed at this very small thickness.

### 4.4 Formation of nanodots formed by PS-PDMS 11,700-2,900

Fig. 9(a) shows SEM images of self-assembled nanopattern using PS-PDMS with the molecular weight of 11,700-2,900 and the corresponding schematic cross-section images of the film height profile before [Fig. 9(b)] and after [Fig. 9(c)] etching process. Fig. 9(a) shows SEM images of nanopatterns when the spin-coating speed was changed to (1) 4000, (2) 6000, and (3) 8000 rpm. All these images were also taken on samples after $O_2$ plasma etching had been conducted on samples. According to our analysis, self-assembled nanodot patterns with diameter and pitch as small as 10 and 20 nm, respectively, were obtained. Similar to the PS-PDMS of 13,500-4,000, the thickness of the PS-PDMS film, which formed before etching process, decreased with the increase of the spin-coating speed. The thickness of the PS-PDMS film significantly decreased when the spin-coating speed increased from 4000 to 6000 rpm. Fig. 9(c) shows the schematic cross-section images of the film height profile after etching process, and the numbers correspond to those of Figs. 9(a) and 9(b).

When the spin-coating speed was 4000 rpm, self-assembled nanodots with diameter and pitch as small as 10 and 20 nm, respectively, were obtained. This result is shown in Fig. 9(a-1). However, the thickness of the PS-PDMS film was 51 nm, which was more than two times the pitch of the nanodots. We believe that two layers of self-assembled nanodots were formed on the surface of the substrate, as described in Fig. 9(b-1). Therefore, the SEM image in Fig. 9(a-1) only shows the first layer of the self-assembled nanodots near the surface of PS-PDMS film as shown in Fig. 9(c-1) since the same condition of RIE was applied on all samples.

When the spin-coating speed was 6000 rpm, the thickness of the PS-PDMS film was 33 nm and self-assembled nanodots were formed. According to our analysis, the diameter and pitch of the nanodots were 10 and 20 nm, respectively. This result is shown in Fig. 9(a-2).

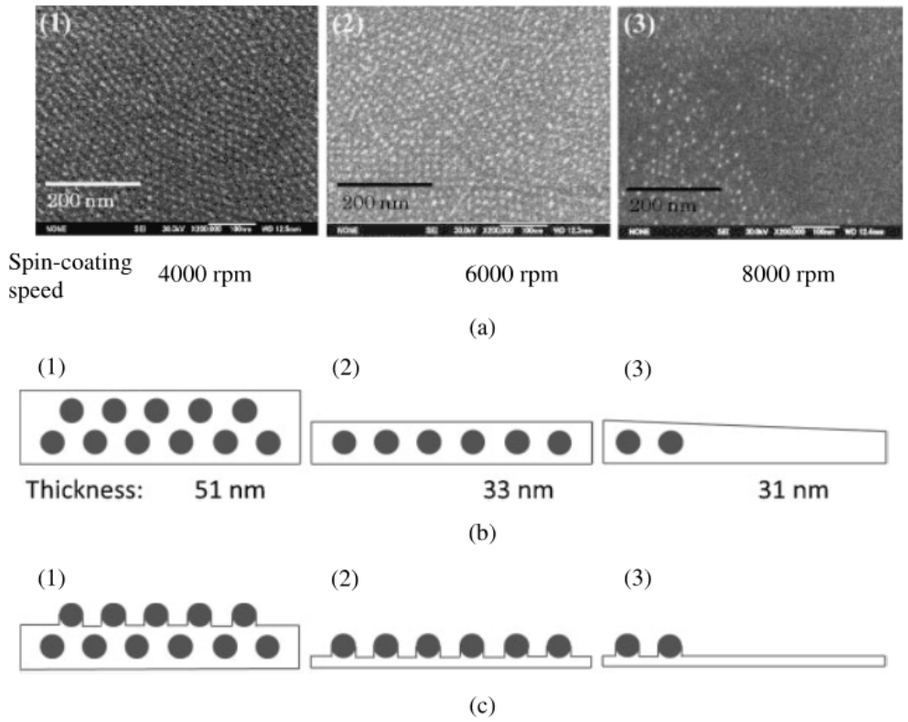


Fig. 9. (a) SEM images of self-assembled nanopatterns using PS–PDMS with the molecular weight of 11,700–2,900. Images (1)–(3) show SEM images of nanopatterns when the spin-coating speed was changed to 4000, 6000, and 8000 rpm, respectively. (b, c) Schematic cross-section images of the correlating film height profile: (b) before etching and (c) after etching.

When the spin-coating speed was 8000 rpm, the thickness of the PS-PDMS film was 31 nm and self-assembled nanodots were arbitrarily formed on the surface of the substrate. The diameter of the nanodots was 10 nm. This result is shown in Fig. 9(a-3).

The self-assembled nanodots were well-formed using PS-PDMS with molecular weight of 11,700-2,900, as shown in Figs. 9(a-1) and 9(a-2). However, nanodots in Fig. 9(a-1) were self-assembled into two layers since the thickness of the PDMS film was double the pitch of the nanodots. Hence, this nanodot pattern would be difficult to be utilized on the pattern transfer. As shown in Fig. 9(a-3), the self-assembled nanodots were partly formed on the surface of substrate. The reason of this is because the thickness of PDMS film is too thin.

According to the results, the pitch of nanodots obtained experimentally is different from our prediction, as shown in Fig. 10. In our experiment, the pitch is directly proportional to the product of $\chi N$, as shown by the dashed line in Fig. 10. This difference is probably caused by two factors. The first is inappropriate value of the segment length and the second is that the microphase-separation condition of used PS-PDMS is not in strong segregation. This graph, however, could be used as a guide in the selection of the molecular weight of PS-PDMS BCP to form the smaller self-assembled nanodots.

According to our experiment result that PS-PDMS with molecular weight of 11,700-2,900 is more stable in forming nanodots than PS-PDMS with molecular weight of 13,500-4,000 due to the value of its PDMS volume fraction, and we describe this phenomenon in mean-field

phase diagram in Fig. 11. We believe that the dotted-line separating between the cylinder-forming PS-PDMS and the sphere-forming PS-PDMS could be drawn near PS-PDMS with molecular weight of 13,500-4,000 because the characteristic of this PS-PDMS is unstable in forming sphere structure and tends to form cylinder. The dashed line separates the order-disordered phase of PS-PDMS. Therefore, the region between the dotted line and the dashed line describes the spherical morphology of PS-PDMS BCP. Fig. 11, however, is important in the selection of the PS-PDMS molecular weight and the minority volume block fraction of PDMS in order to form the desired nanopattern. Therefore, it is necessary to adopt PS-PDMS with minority volume block fraction of PDMS that is smaller than 24% to obtain nanodots pattern according to our experimental result.

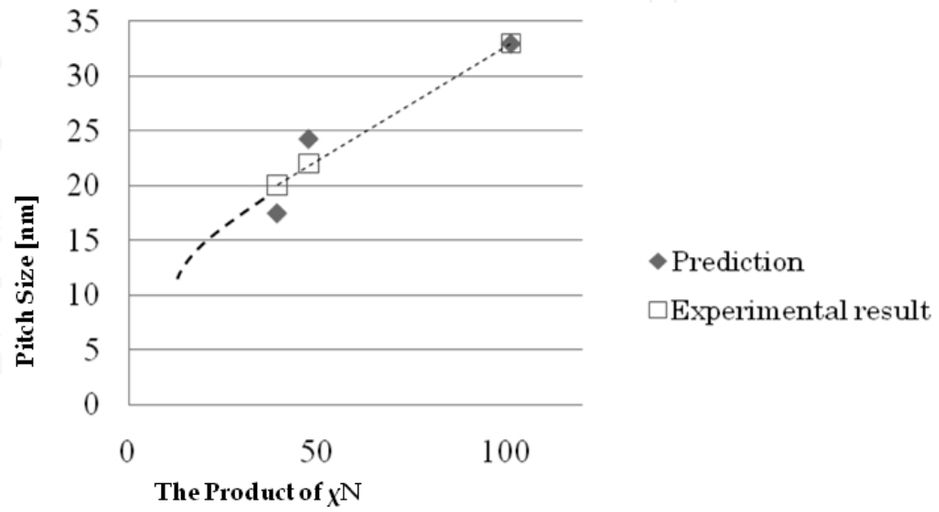


Fig. 10. A graph of the pitch sizes of nanodots according to prediction and experimental results.

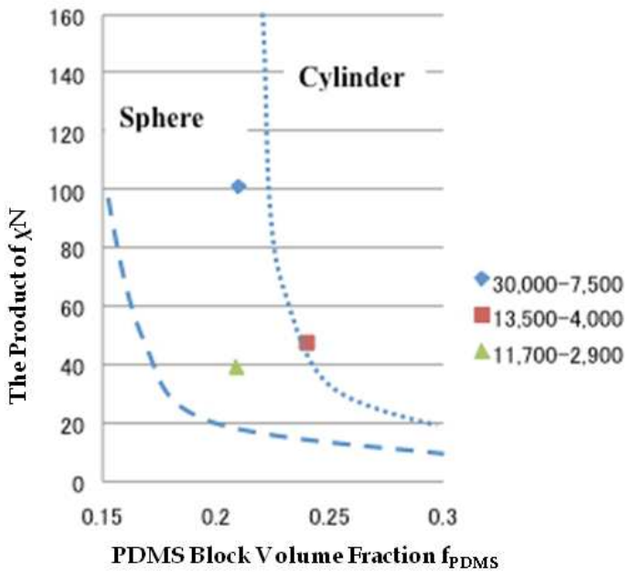


Fig. 11. The position of our adopted PS–PDMS in mean-field phase diagram for BCP melts.

We have succeeded in fabricating self-assembled nanodots with a diameter as small as 10 nm and a pitch size as small as 20 nm using PS-PDMS with molecular weight of 11,700-2,900. Those nanodots were able to form on a large area, which was confirmed by randomly imaging the surface of a 1 $cm^2$ sample using SEM. However, PS-PDMS with molecular weight of 11,700-2,900 is more stable in forming nanodots than PS-PDMS with molecular weight of 13,500-4,000 due to the value of its PDMS fraction. The nanodot size promises for fabricating 1.86 Tbit/$in.^2$ storage device using patterned media method by ease process and low cost fabrication. It is advantageous that the gap between nanodots is the same as the nanodot size, as this will reduce the effect of instability from thermal fluctuation.

## 5. Conclusion

We have succeeded in fabricating self-assembled nanodots using PS-PDMS with molecular weights of 30,000-7,500, 13,500-4,000, and 11,700-2,900. By optimizing the concentration and the dropped volume of PS-PDMS solution, nanodots with a diameter as small as 23 nm and a pitch size as small as 33 nm were formed using PS-PDMS with molecular weights of 30,000-7,500. These indicate that the concentration and the dropped volume of PS-PDMS solution play role on the formed nanopattern size.

Nanodots with a diameter as small as 12 nm and a pitch size as small as 22 nm were formed using PS-PDMS with molecular weights of 13,500-4,000, and nanodots with a diameter as small as 10 nm and a pitch size as small as 20 nm using PS-PDMS with molecular weight of 11,700-2,900. The latter nanodot size is promising for fabrication 1.86 Tbit/$in.^2$ storage device because of its high possibility to be used as mask for subtractive transfer process. In experiment, we found that an optimum thickness of the PS-PDMS film is required to obtain self-assembled nanadots on large areas especially when the position of the BCP is not in stable area in mean-field phase diagram for BCP melts. The optimum thickness could be obtained simply by adjusting the spin-coating speed during formation of the thin block copolymer film. We have predicted the limitations in the selection of PS-PDMS BCP to be used in forming smaller sizes of self-assembled nanodots of this BCP. In order to increase the possibility of applying this technique to nano-electronic devices, we plan on further reducing the nanodot size and controlling the orientation of nanodots in the future.

## 6. Acknowledgment

This work was funded by the New Energy and Industrial Technology Development Organization (NEDO) under the development of nanobit technology for the ultrahigh density magnetic recording (Green IT) project. We gratefully thank Prof. K. Itoh from Graduate School of Engineering, Gunma University, for the use of RIE tool.

## 7. References

Huda, M.; Yin, Y. & Hosaka, S. (2010) Self-assembled nanodot fabrication by using diblock Copolymer. *Key Eng. Mater. AMDE,* Vol. 459, pp. 120-123, ISSN 1662-9795

Huda, M.; Akahane, T.; Tamura, T.; Yin, Y. & Hosaka, S. (2011) Fabrication of 10-nm-order block copolymer self-assembled nanodots for high-density magnetic recording. *Jpn. J. Appl. Phys.,* Vol. 50, pp. 06GG06-1 - 06GG06-5, ISSN 1347-4065

Hosaka, S.; Zulfakri, B. M.; Shirai, M.; Sano, H.; Yin, Y.; Miyachi, A. & Sone, H. (2008) Extremely small proximity effect in 30 keV electron beam drawing with thin calixarene resist for 20×20 nm² pitch dot arrays. *Appl. Phys. Express,* Vol. 1, pp. 027003-027005, ISSN 1882-0786

Hieda, H.; Yanagita, Y.; Kikitsu, A.; Maeda, T. & Naito K. (2006) Fabrication of FePt patterned media with diblock copolymer templates. *J. Photopolym. Sci. Technol*. Vol. 19, No. 3, pp. 425-430, print: ISSN 0914-9244, online: ISSN 1349-6336

Matsen, M. W. & Schick, M. (1994) Stable and unstable phases of a diblock copolymer melt. *Phys. Rev. Lett.*, Vol. 72 pp. 2660–2663, print: ISSN 0031-9007, online: ISSN 1079-7114

Ross, C. A. et al. (2008) Si-containing block copolymers for self-assembled nanolithography. *J. Vac. Sci. Technol. B*. Vol. 26, pp. 2489-2494, print: ISSN 1071-1023, online: ISSN 1520-8567

Bita, I.; Yang, J. K. W.; Jung, Y. S.; Ross, C. A.; Thomas, E. L.; & Berggren, K. K. (2008) Graphoepitaxy of Self-Assembled Block Copolymers on Two-Dimensional Periodic Patterned Templates. *Science*, Vol. 321, pp. 939-943, print: ISSN 0036-8075, online: ISSN 1095-9203

Knoll, A.; Horvat A.; Lyakhova, K. S.; Krausch, G.; Sevink, G. J. A.; Zvelindovsky, A. V. and Magerle R. (2002) Phase Behavior in Thin Films of Cylinder-Forming Block Copolymers. *Phys. Rev. Lett.*, Vol. 89, pp. 035501-035504, print: ISSN 0031-9007, online: ISSN 1079-7114

Bates, F. S. & Fredrickson, G. H. (1990) Block Copolymer Thermodynamics: Theory and Experiment. *Annu. Rev. Phys. Chem.,* Vol. 41, pp. 525-557, ISSN 0066-426X

Aissou, K.; Kogelschatz, M.; Baron, T. and Gentile, P. (2007) Self-assembled block polymer templates as high resolution lithographic masks. *Surf. Sci.* Vol. 601, pp. 2611-2614, ISSN 00396028


**State-of-the-Art of Quantum Dot System Fabrications**

Edited by Dr. Ameenah Al-Ahmadi

ISBN 978-953-51-0649-4
Hard cover, 172 pages
**Publisher** InTech
**Published online** 13, June, 2012
**Published in print edition** June, 2012

The book "State-of-the-art of Quantum Dot System Fabrications" contains ten chapters and devotes to some of quantum dot system fabrication methods that considered the dependence of shape, size and composition parameters on growth methods and conditions such as temperature, strain and deposition rates. This is a collaborative book sharing and providing fundamental research such as the one conducted in Physics, Chemistry, Material Science, with a base text that could serve as a reference in research by presenting up-to-date research work on the field of quantum dot systems.

**How to reference**

In order to correctly reference this scholarly work, feel free to copy and paste the following:

Miftakhul Huda, You Yin and Sumio Hosaka (2012). Self-Assembled Nanodot Fabrication by Using PS-PDMS Block Copolymer, State-of-the-Art of Quantum Dot System Fabrications, Dr. Ameenah Al-Ahmadi (Ed.), ISBN: 978-953-51-0649-4, InTech, Available from: http://www.intechopen.com/books/state-of-the-art-of-quantum-dot-system-fabrications/self-assembled-nanodot-fabrication-by-using-ps-pdms-block-copolymer

INTECH
open science | open minds

**InTech Europe**
University Campus STeP Ri
Slavka Krautzeka 83/A
51000 Rijeka, Croatia
Phone: +385 (51) 770 447
Fax: +385 (51) 686 166
www.intechopen.com

**InTech China**
Unit 405, Office Block, Hotel Equatorial Shanghai
No.65, Yan An Road (West), Shanghai, 200040, China
中国上海市延安西路65号上海国际贵都大饭店办公楼405单元
Phone: +86-21-62489820
Fax: +86-21-62489821

IntechOpen